processes

MDPI

Article

From Structure to Efficiency: Unveiling the Role of Calcination Temperature in Nb_2O_5-Based DSSCs

Ronald Luiz Castiglioni Davi [1], Edson Araujo de Almeida [2], Ana Paula Peron [3], Everson do Prado Banczek [4], Osvaldo Valarini Junior [5] and Gideã Taques Tractz [6,*]

[1] Chemical Engineering Course, Federal Technological University of Paraná-UTFPR-CM, Campo Mourão 87301-899, Paraná, Brazil; ronaldluiz@alunos.utfpr.edu.br
[2] Graduate Program in Chemistry, State University of Maringá-UEM, Maringá 87020-900, Paraná, Brazil; edsonalmeida2009@gmail.com
[3] Department of Biodiversity and Nature Conservation, Federal Technological University of Paraná-UTFPR-CM, Campo Mourão 87301-899, Paraná, Brazil; anaperon@utfpr.edu.br
[4] Chemistry Department, Central Western State University, Guarapuava 3629-8100, Paraná, Brazil; ebanczek@unicentro.br
[5] Department of Food and Chemical Engineering, Federal Technological University of Paraná-UTFPR-CM, Campo Mourão 87301-899, Paraná, Brazil; osvaldovalarini@utfpr.edu.br
[6] Department of Chemistry, Federal Technological University of Paraná-UTFPR-CM, Campo Mourão 85884-000, Paraná, Brazil
* Correspondence: gideatractz@utfpr.edu.br; Tel.: +55-42-999805634

Abstract: The development of dye-sensitized solar cells (DSSCs) has gained prominence as an economical alternative for photovoltaic energy conversion. This work investigates the synthesis of niobium pentoxide (Nb_2O_5) by the Pechini method, followed by calcination at different temperatures (500 °C, 600 °C and 700 °C) to evaluate its structural, morphological, and electrochemical properties as a photoanode material in DSSCs. SEM and XRD analyses revealed that calcination at 600 °C produced a material with optimized particle size (642.17 ± 37 nm) and adequate crystalline structure, favoring dye adsorption and electronic transport. Electrochemical characterization, including open-circuit potential and impedance spectroscopy, indicated that the sample at 600 °C presented superior photovoltaic performance, achieving a power conversion efficiency of 1.39% and electron lifetime equal to 0.159 s. These findings suggest that Nb_2O_5, under controlled calcination conditions, may act as a promising alternative to TiO_2 substitution in DSSC applications.

Keywords: grätzel cell; pechini; solid state electrochemistry; renewable energy

check for updates

Academic Editors: Mohammad Istiaque Hossain, Brahim Aïssa and Amith MD. Abdullah Khandakar

Received: 21 May 2025
Revised: 9 June 2025
Accepted: 10 June 2025
Published: 12 June 2025

Citation: Davi, R.L.C.; Almeida, E.A.d.; Peron, A.P.; Banczek, E.d.P.; Junior, O.V.; Tractz, G.T. From Structure to Efficiency: Unveiling the Role of Calcination Temperature in Nb_2O_5-Based DSSCs. *Processes* **2025**, *13*, 1857. https://doi.org/10.3390/pr13061857

Copyright: © 2025 by the authors. Licensee MDPI, Basel, Switzerland. This article is an open access article distributed under the terms and conditions of the Creative Commons Attribution (CC BY) license (https://creativecommons.org/licenses/by/4.0/).

1. Introduction

The intensification of pollution, depletion of natural resources, and the acceleration of the greenhouse effect have significantly aggravated environmental concerns in recent years. In this context, photovoltaic systems have emerged as a promising alternative for sustainable energy generation, drawing increasing attention to renewable and low-emission energy sources. Among various photovoltaic technologies, dye-sensitized solar cells (DSSCs) stand out due to their low production cost, simple fabrication process, and potential application in flexible devices, making them an attractive option for clean energy conversion [1,2].

DSSCs use a dye to absorb light and generate electrons, which are transferred to a semiconductor, usually titanium oxide (TiO_2), where charge separation occurs [3]. Despite its low cost and chemical stability, TiO_2 has limitations such as a wide band gap (~3.2 eV),

which restricts absorption to ultraviolet light, and low electrical conductivity, which requires structural modifications or doping to improve its performance. Similarly, the use of new materials such as niobium pentoxide (Nb_2O_5) [4], zinc oxide (ZnO) [5], and cerium oxide (CeO_2) [6], among others, is promising, as they present limitations and customized properties that can be easily modified by synthetic routes.

Because of its structural and electrical characteristics, Nb_2O_5 has sparked interest in materials research for solar devices [7]. Niobium (Nb) in oxide form can play a role as a dopant when added to semiconductor oxides like TiO_2, encouraging the creation of intermediate electronic states in the forbidden band gap and favoring visible light absorption [8]. Doping the material can enhance its electrical conductivity, reducing charge transfer resistance and minimizing electronic recombination. Similarly, Nb_2O_5 has advantages over TiO_2, not only related to the production cost, but also in morphology and electronic properties [8].

Beyond their role in DSSCs, metal oxides are also extensively utilized in perovskite-based solar cells and related optoelectronic devices [9–11]. Perovskite materials often incorporate oxide layers that serve as charge transport or blocking layers, benefiting from the stability and tunable properties of metal oxides. These oxides, such as TiO_2 and Nb_2O_5, have been widely studied for their ability to improve device performance by enhancing charge extraction and reducing recombination losses [9,12]. While perovskites themselves show outstanding light absorption and charge carrier properties, challenges related to stability and toxicity persist [13,14]. Thus, metal oxides continue to be essential components in the quest for more efficient and durable photovoltaic technologies, offering robustness and adaptability through various synthesis methods.

There are various ways to synthesize these charge transport materials, but one of the most popular methods for producing metal oxides with excellent purity and morphological control is the Pechini pathway [15]. This process creates a polymeric precursor in which a carboxylic acid, like citric acid, chelates the metal ions, and then a polyol alcohol, like ethylene glycol, polymerizes them. The polymeric precursor is transformed into metal oxides with certain structural properties for photovoltaic applications during calcination. This temperature could influence the crystal morphology, structure, and tailor the performance of the material when applied in several areas [15].

The objective of this work is to synthesize Nb_2O_5 using the Pechini methodology, with calcination at different temperatures, analyzing the material structurally and morphologically, with subsequent application in a photovoltaic device.

2. Materials and Methods

Nb_2O_5 particles were prepared by Pechini methodology as follows: an amount of 79.2 g of citric acid was dissolved in 300 mL of ethylene glycol, under stirring at 70 °C until complete solubilization. Then, 6.22 g of ammonium niobium complex, provided by CBMM (Companhia Brasileira de Metalurgia e Mineração, Araxá, Minas Gerais, Brazil), was inserted, and the temperature was increased to 100 °C [4]. The resin formed was calcinated for 4 h, at temperatures of 500 °C, 600 °C, and 700 °C with a puff deagglomeration at 400 °C. The production of Nb_2O_5 is illustrated in the flowchart in Figure S1 in Supplementary Information.

The synthesized powders were evaluated by XRD diffraction, using D2 phaser Bruker equipment (using $Cu_{K\alpha}$ radiation source with a wavelength of 0.1506 nm operated at 30 kV and 10 mA), and by light dynamic scattering using Litesizer 500 and Anton PAAR equipment, coupled with a Zeta potential analyzer (in deionized water solution). Scanning Electron Microscopy, using Tescan Vega Microscopy, was also performed, with magnification of 500× for morphological characterization. The energy band gap of oxides was

calculated using UV-Vis spectra of samples, obtained in UV-VIS-NIR, Plus Shimadzu, using the Kubelka–Munk method, described in Equation (S1) of the Supplementary File [6].

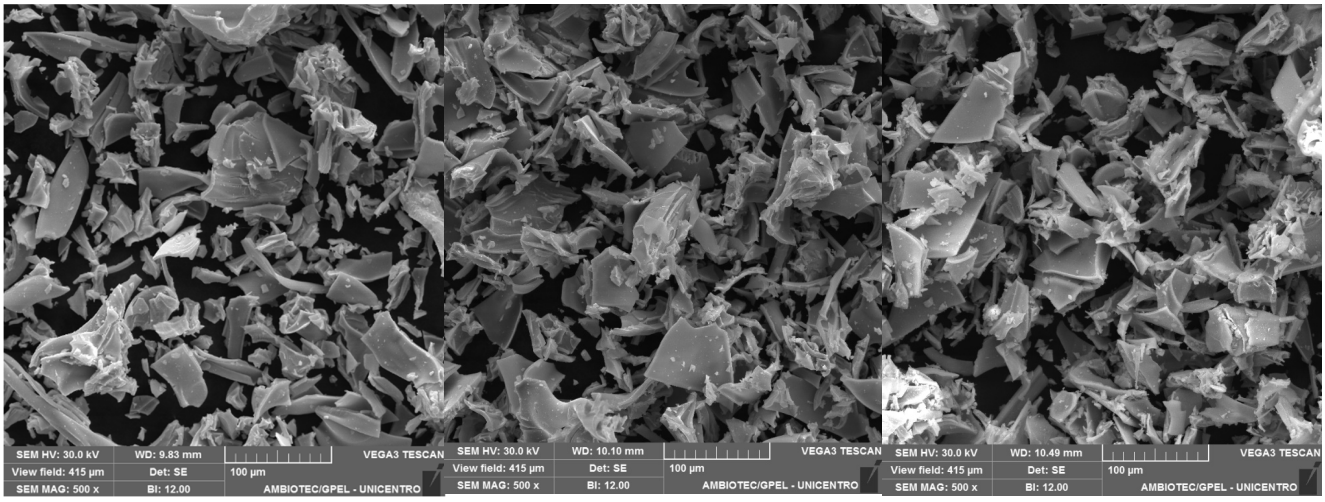
Nb_2O_5 paste was prepared as follows: an amount of 3 g of Nb_2O_5 was mixed with 0.1 mL of acetyl acetone, 0.1 mL of Triton-X, 0.1 mL of polyethylene glycol, and 3 mL of deionized water, under maceration for 30 min [16–18]. The paste was coated under a fluorine-doped tin oxide surface (FTO; 7 Ω sq^{-1} Aldrich®) by the doctor blading method. Films were sintered for 30 min at 450 °C and impregnated with N719 dye solution in ethanol (1×10^{-4} mol L^{-1}) for 24 h.

Solar cells with an active area of 0.2 cm^2 were assembled in sandwich format, using the anode (Nb_2O_5 + dye) with a counter electrode produced using platinum (Pt) [18]. The charge remediation was made by iodine electrolytes [18]. The techniques employed to electrochemically characterize DSSC were the open-circuit curves, j-V curves, and Electrochemical Impedance Spectroscopy (EIS) (0.01–1 kHz with 10 mV of amplitude). These techniques were employed in a Zhenium Zahner potentiostat, coupled with the Xe lamp at 100 mW cm^{-2} under 1.5 AM irradiation.

3. Results and Discussion

3.1. Morphological and Structural Characterization

In Figure 1, the SEM micrographs for Nb_2O_5 particles produced are depicted.



(**A**) (**B**) (**C**)

Figure 1. SEM micrographs of Nb_2O_5 particles produced by Pechini methodology at 500 °C (**A**), 600 °C (**B**), and 700 °C (**C**).

Micrographs obtained by Scanning Electron Microscopy (SEM) of Nb_2O_5 synthesized by Pechini methodology at different temperatures show specific morphological characteristics that can be correlated with the synthesis conditions. In general, the samples presented an irregular morphology, with a marked presence of agglomerates, which is in accordance with the literature for the Pechini methodology [19].

Irregular morphology is particularly interesting for applications in emergent photovoltaic systems, since the rough surfaces and high surface area enhance the dye-sensitized adsorption [20,21]. In addition, these results may also be exploited in other areas, as pollutant adsorption, providing a greater capacity for interaction with the target species.

The analysis of the particle size distribution (Figures S2–S4 in Supplementary Information) indicated a predominance in the range of 20–40 µm, with better homogeneity observed in the samples treated at 500 °C and 600 °C. On the other hand, the sample calcined at 700 °C exhibited a higher concentration of particles around the 20 µm size range. This

can be attributed to an enhanced sintering process at this temperature, promoting particle coalescence and growth, resulting in larger and denser agglomerates. This behavior is consistent with the observed increase in average particle size, reflecting the thermal-driven grain growth and particle fusion at higher calcination temperatures. To analyze the particles in suspension, Dynamic Light Scattering was performed, with Zeta potential analysis, as depicted in Table 1.

Table 1. Particle size and zeta potential under ethanol solution of Nb_2O_5 particles produced by Pechini methodology at 500 °C, 600 °C, and 700 °C.

Temperature (°C)	Particle Size Diameter (nm)	Zeta Potential (mV)
500	827.63 ± 26	−25.53 ± 2.84
600	642.17 ± 37	−8.27 ± 0.32
700	1022.57 ± 46.8	−20.43 ± 1.33

The analysis of particle size and zeta potential values corroborates these observations. It can be observed that the sample treated at 500 °C presented an average diameter of 827.63 ± 26 nm and a zeta potential of −25.53 ± 2.84 mV, indicating the formation of intermediate-sized particles with good colloidal stability due to the high negative value of zeta potential. The sample at 600 °C presented a reduced diameter of 642.17 ± 37 nm and a lower superficial charge, when compared to the others, suggesting a decrease in colloidal stability with a higher propensity to agglomerate formation [22]. Since the organic residues were rapidly burned without a heating ramp, between 500 °C and 600 °C, it is indicated that the powder initially undergoes fragmentation due to the release of gases such as H_2O and CO_2 (reducing the apparent particle size), followed by particle rearrangement as they begin to fuse and sinter, thus not following the expected trend of increasing particle size with temperature.

The sample calcinated at 700 °C showed a significant increase in particle size, reaching 1022.57 ± 46.8 nm, which can be attributed to more intense sintering at high temperatures, resulting in larger particles and denser agglomerates. It is important to emphasize that larger particles tend to reduce the active surface area available for the adsorption of dyes, decreasing the efficiency in solar energy conversion [23]. On the other hand, rough surfaces and heterogeneous particle distribution can still enhance the adsorption, as seen in those treated at lower temperatures.

X-ray diffraction of the Nb_2O_5 samples synthesized via the Pechini method and calcinated at several temperatures is presented in Figure 2.

The diffraction patterns show restricted and well-defined peaks in the same 2θ regions, indicating the formation of crystalline materials. The absence of significant deviation or emergence of new peaks suggests that there was no phase transition between the observed temperatures. The identification of the crystalline planes was performed using Crystallographica® software (Version 3.1), allowing the cataloging of the peaks and the determination of (001), (180), and (181) planes, characteristic of the orthorhombic phase of Nb_2O_5 [4,7]. These findings reinforce the stability of the crystalline structure under the conditions tested, and are relevant for the application of materials such as photoanodes in solar systems. To evaluate the average crystal size, the Scherrer equation (Equation (1)) was applied, considering the most intense peak in each sample [7].

$$D = (K\lambda)/B(\cos\theta) \quad (1)$$

With D representing the crystallite size, K is the Scherrer constant (K = 0.9), λ the wavelength of X-rays, B the FWHM of the diffraction peak, and θ the Bragg angle. Using

Equation (1), the values of 12.26 nm, 14.39 nm, and 18.51 nm were obtained for powders sintered at 500 °C, 600 °C, and 700 °C, respectively. In essence, a progressive increase in crystallite size is observed with increasing temperature, which is associated with the growth of the crystalline domains. These values are in agreement with those reported by Eblagon et al. [24] for Nb_2O_5 synthesis and present a particularly interesting behavior for DSSC use, since adequate control of crystalline size can also influence the surface area available for dye adsorption, impacting the photoconversion energy efficiency of the device.

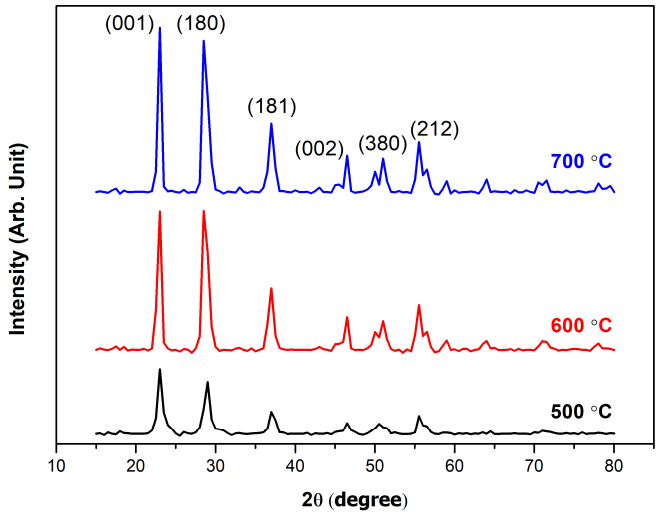


Figure 2. XRD patterns of Nb_2O_5 particles produced by Pechini methodology at 500 °C, 600 °C, and 700 °C.

3.2. Electrochemical Device Characterization

Open-circuit potential (V_{oc}) tests were performed under conditions with and without illumination, in order to evaluate the photosensitivity of the DSSC device constructed with Nb_2O_5 as the electron transport material (Figure 3).

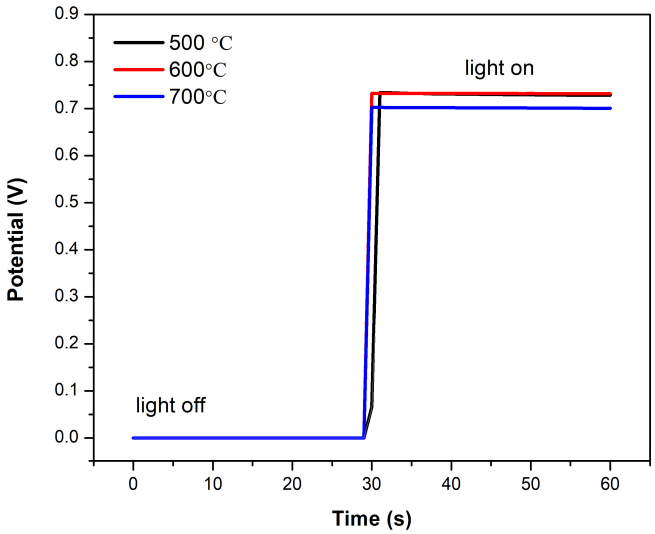


Figure 3. Open-circuit potential curves for DSSC produced with Nb_2O_5 particles calcinated at 500 °C, 600 °C, and 700 °C.

In the absence of light, the potential recorded was close to 0 V, confirming the absence of photosensitive activity. With the application of light, V_{oc} increased significantly, reaching a value of approximately 0.7 V [25]. This value is considered promising when

compared to TiO_2, which generally presents open-circuit potentials in the same range (~0.7 V), demonstrating the viability of Nb_2O_5 as a potential replacement for DSSCs [25].

The formation of the open-circuit potential is closely related to the difference between the Fermi level of the semiconductor and the redox potential of the electrolyte used [26]. The results obtained indicate that the conduction band of Nb_2O_5 is adequately positioned for the injection of electrons from the dye to the semiconductor, favoring the charge separation process. Furthermore, the V_{oc} values recorded for the powders calcined at different temperatures did not show significant variations, suggesting that the conduction band position remained stable regardless of the increase in crystallite size or material crystallinity, according to a gap value of 2.92 eV (Figure S5 in Supplementary Information), obtained with no variation for all samples [4]. The direct band gap was calculated, according to the approach for Nb_2O_5 reported by several studies in the literature, highlighting the relevance of this type of transition in various experimental and structural contexts [27–29]. This stability is a positive factor for future applications of Nb_2O_5 in dye-sensitized solar cells and other emergent photovoltaic applications. On the other hand, the current produced in the device is significantly influenced by particle properties, such as microstructure, electron diffusion length, charge recombination, porosity, and dye loading. Therefore, j-V curves were created for solar cells and are depicted in Figure 4.

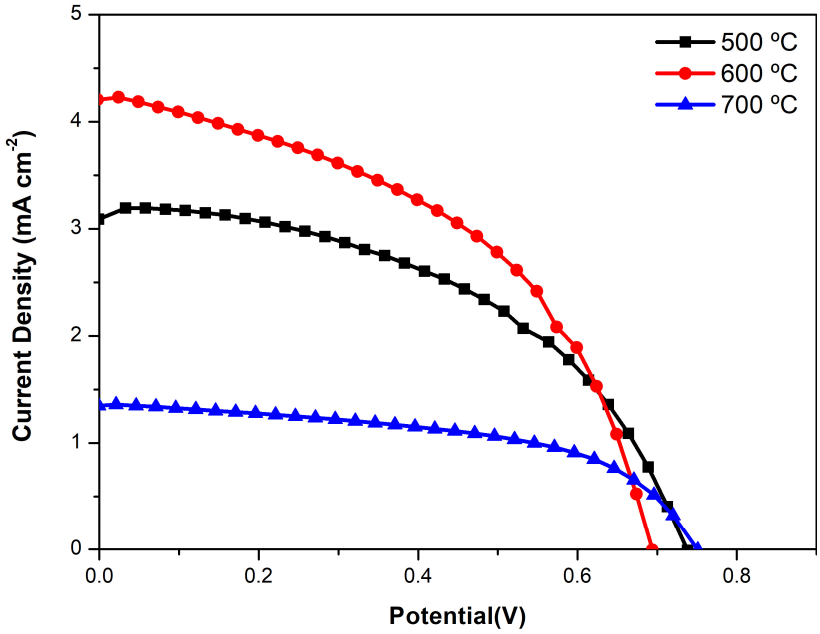


Figure 4. j-V curves for DSSC produced with Nb_2O_5 particles calcinated at 500 °C, 600 °C, and 700 °C.

As can be seen in Figure 4, the cell produced at 600 °C presented the highest current density, resulting in a larger area under the curve, which is directly reflected in a higher photovoltaic efficiency (PCE). Using Equation (2), PCE could be calculated, with maximum values of current density (Jsc), potential (V_{oc}), and Fill Factor (FF), providing a more accurate indication of the energy conversion capacity of the photovoltaic device [30].

$$PCE = (J_{sc} \times V_{oc} \times FF/P_{in}) \quad (2)$$

Analyzing the results in Table 2, the cell produced with Nb_2O_5 at 600 °C showed better PCE, equal to 1.39%. This performance is mainly associated with the higher current density obtained, which can be related to the smaller particle size observed to this sample, resulting in an increase in the specific surface area and, consequently, in a greater number

of sites available for dye adsorption [31,32]. On the other hand, the sample calcined at 700 °C, despite presenting the highest Fill Factor (0.536), presented the lowest efficiency (0.55%), possibly due to the larger crystallite size (18.51 nm) and the consequent reduction in the surface area available for dye adsorption. The sample calcined at 500 °C presented an intermediate behavior, with an efficiency of 1.13%. The short-circuit current density (Jsc) values presented in Table 2 reveal a clear dependence on the calcination temperature. An increase from 3.19 mA cm^{-2} at 500 °C to 4.23 mA cm^{-2} at 600 °C indicates enhanced charge transport and reduced recombination, likely due to the improved crystallinity and interconnectivity of the TiO_2 particles. However, a subsequent decrease to 1.36 mA cm^{-2} at 700 °C suggests that excessive grain growth may hinder dye adsorption and reduce the effective surface area, ultimately reducing photocurrent generation.

Table 2. Photovoltaic parameters for DSSC prepared with Nb_2O_5 particles calcinated at 500 °C, 600 °C, and 700 °C.

Temperature (°C)	J_{sc} (mA cm^{-2})	V_{oc} (V)	FF	PCE (%)
500	3.19	0.738	0.481	1.13
600	4.23	0.694	0.474	1.39
700	1.36	0.751	0.536	0.55

DSSC was prepared using N719 as a dye in ethanolic solution (1×10^{-4} M), with a Pt electrode and an iodine-based electrolyte. The incident power was 100 mW cm^{-2}.

These results are promising, considering that oxide substitutes for TiO_2 rarely achieve higher efficiencies. For instance, SnO_2 in nanoparticulate form typically exhibits efficiencies in energy conversion around 0.9% [33], while ZnO reaches approximately 0.57% [34]. Nb_2O_5 when combined with other oxides can enhance the system efficiency, reaching values in the range of 1–2%, and is also highly effective in the fabrication of counter electrodes [35,36]. Similarly, the oxides developed and studied here may act as enhancers for the underlying layers of other materials, creating a synergistic effect. It is also noteworthy that the systems developed in this study do not include an electron-blocking layer using $TiCl_4$ or an efficient sealing mechanism, which could further boost the obtained values. To gain a deeper understanding of the mechanisms involved in charge transfer and recombination processes within the solar cell, it is essential to examine not only the overall performance through j-V curves but also the dynamics of the internal interfaces of the device [37]. In this context, Electrochemical Impedance Spectroscopy (EIS) was applied, as shown in Figure 5.

The analysis of the EIS curves performed on the dye-sensitized Nb_2O_5 system, as shown in Figure 5, reveals crucial information about the charge transfer and recombination processes that occur at the solar cell interfaces [38]. The Nyquist diagram shown in Figure 5 highlights the presence of a capacitive arc at high frequencies, related to the behavior of the counter electrode, which responds to short relaxation times [17]. This behavior is typical of dye-sensitized systems, in which charge transfer occurs rapidly at the device interfaces.

In addition, a distinct capacitive behavior is observed at high frequencies, with the variation associated with the calcination temperature of the Nb_2O_5. This phenomenon corroborates the hypothesis that the calcination process directly influences the charge transfer processes that occur at the working electrode interface [39]. The change in the capacitive arc as the calcination temperature increases is a clear indication that the material microstructure and surface characteristics are being modified, altering the charge transfer behavior in the system.

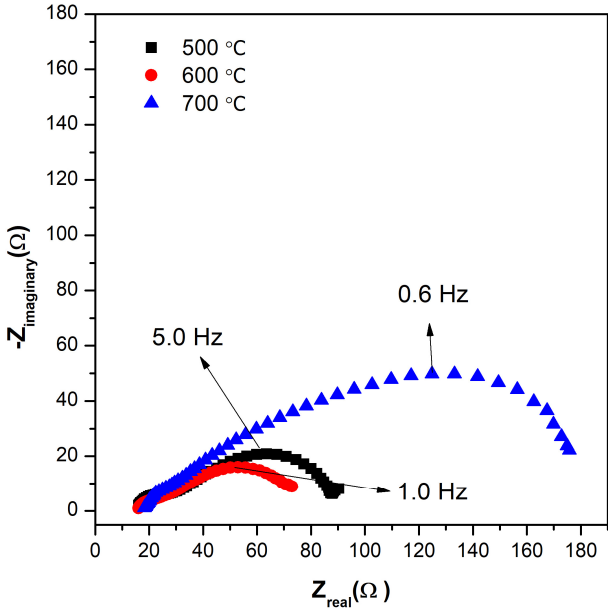


Figure 5. EIS Nyquist diagram for DSSC produced with Nb_2O_5 particles calcinated at 500 °C, 600 °C, and 700 °C.

Specifically, for the systems produced at calcination temperatures of 600 °C, high conductivity and facility in redox reactions were observed, compared to the other systems. These results are consistent with the electrochemical data obtained for the cell current, which indicate greater efficiency in redox reactions and a significant reduction in the system resistance [40]. This improvement in charge transport properties can be attributed to the formation of a structure more favorable to electrical conduction, possibly due to greater surface activation and better crystalline organization of the Nb_2O_5 calcined at 600 °C [23]. In addition, with the fitted Nyquist diagram and the equivalent circuit used, Table 3 and Figures S6–S8 in Supplementary Information provide information on the solar cell resistance interfaces.

Table 3. Solar cell resistances produced with Nb_2O_5 in different temperatures, obtained by Nyquist fitted diagram.

Temperature (°C)	R_S (Ω)	R_{CT} (Ω)	R_{CE} (Ω)
500	41.9	305.0	84.7
600	13.5	66.4	349.0
700	6.57	736.0	246.0

R_{CT} represents charge transport resistance; R_S represents series resistance; and R_{CE} represents counter electrode resistance.

On the other hand, the oxide produced at 500 °C presented intermediate resistances of charge transportation (R_{CT} = 305.0 Ω), evidencing less efficient performance compared to the system calcined at 600 °C (R_{CT} = 66.4 Ω). This suggests that the calcination temperature of 500 °C does not favor the formation of ideal microstructural features for charge transfer, resulting in less efficient electrochemical behavior. Similarly, the system calcined at 700 °C showed high resistances (R_{CT} = 736.0 Ω), which indicates a reduction in the efficiency of charge transfer, possibly due to the higher crystallite size, which may affect the formation of defects in the structure that hinder redox reactions [23].

Using Equation (3), it is possible to calculate τ_e, the electron lifetime (with f representing the frequency of the middle semicircle) [4,41].

$$\tau_e = 1/2\pi f \quad (3)$$

The τ_e results indicate that the electronic lifetime increases with increasing calcination temperature. For the system calcined at 500 °C, the electronic lifetime is 0.031 s, which reflects a rapid recombination of the charge carriers [42–44]. In contrast, the system calcined at 600 °C presents an electronic lifetime of 0.159 s, indicating a slower recombination and, therefore, a higher charge transfer efficiency. The system calcined at 700 °C, with τ_e of 0.265 s, suggests an even slower recombination, but as observed in the impedance curves, this improvement is not accompanied by an increase in the overall efficiency of the system, due to the increase in resistances associated with this calcination process [40,45]. Although an increase in electron lifetime (τ_e) was observed with higher calcination temperatures, this parameter alone does not ensure improved device efficiency. The overall performance also depends on how effectively the photogenerated electrons are collected, which is governed by the electron collection time. In cases where the material becomes more compact or loses surface area, as observed in particles produced at 700 °C, electron transport may be hindered, reducing collection efficiency despite the longer τ_e. A proper evaluation of charge collection dynamics requires techniques such as Intensity-Modulated Photocurrent Spectroscopy (IMPS), which were not employed in the present study [18].

These data confirm that the calcination temperature is a critical parameter in modulating the electrochemical properties of the dye-sensitized Nb_2O_5 system. Impedance and electronic lifetime analysis provide a detailed understanding of charge transport mechanisms and the effects of calcination temperature on solar cell interfaces.

4. Conclusions

The synthesis of Nb_2O_5 by the Pechini method proved to be an effective way to obtain particles with adjustable morphology and structural characteristics by controlling the calcination temperature. The results obtained indicate that increasing the temperature promotes the growth of crystalline domains and the formation of large agglomerates, as observed by SEM images and XRD measurements. On the other hand, calcination at 600 °C showed an intermediate behavior, with particles of reduced size (642.17 $\pm$ 37nm) and a relatively homogeneous surface.

Electrochemical measurement of the dye-sensitized solar cells revealed that the material calcinated at 600 °C produced a higher photoconversion energy efficiency (PCE = 1.39%). Electrochemical impedance spectroscopy reinforced the conclusion, with particles produced at intermediate temperatures having reduced charge transfer resistance and an electron lifetime of 0.159 s, which is supposed to be related to the morphology, electrical conductivity, and surface area for dye adsorption.

To enhance the overall efficiency of the DSSC, future work could focus on improving dye adsorption through surface functionalization of the Nb_2O_5 particles, engineering the photoanode architecture to increase surface area and light scattering, and incorporating co-sensitizers or conductive additives to facilitate charge transport and reduce recombination losses.

Supplementary Materials: The following supporting information can be downloaded at: https://www.mdpi.com/article/10.3390/pr13061857/s1. Figure S1: Flowchart diagram of Nb_2O_5 process production by Pechini methodology; Figure S2: Particle distribution to Nb_2O_5 calcinated at 500 °C; Figure S3: Particle distribution to Nb_2O_5 calcinated at 600 °C; Figure S4: Particle distribution to Nb_2O_5 calcinated at 700 °C; Figure S5: Gap estimated by Kubelka–Munk method to Nb_2O_5 studied. Figure S6: Equivalent circuit used to fit EIS Nyquist diagram to dye-sensitized solar cells in A, with fitted diagram in B to Nb_2O_5 produced at 500 °C; Figure S7: Equivalent circuit used to fit EIS Nyquist diagram to dye-sensitized solar cells in A, with fitted diagram in B to Nb_2O_5 produced at 600 °C.; Figure S8: Equivalent circuit used to fit EIS Nyquist diagram to dye-sensitized solar cells in A, with fitted diagram in B to Nb_2O_5 produced at 700 °C.

Author Contributions: R.L.C.D.: conceptualization, methodology, formal analysis, resources, writing—review and editing, supervision; E.A.d.A.: conceptualization, methodology, formal analysis, writing—original draft preparation, visualization; A.P.P.: formal analysis, investigation, data curation, project administration; E.d.P.B.: validation, data curation, writing—original draft preparation; O.V.J.: investigation, supervision, project administration; G.T.T.: conceptualization, methodology, formal analysis, validation, investigation, project administration, writing—original draft preparation, funding acquisition. All authors have read and agreed to the published version of the manuscript.

Funding: This research received no external funding.

Data Availability Statement: The original contributions presented in this study are included in the article/supplementary material. Further inquiries can be directed to the corresponding author.

Acknowledgments: The authors are grateful to UNICENTRO and UEM for all the electrochemical and organic analyses. The authors would like to thank the Multiuser Laboratory of Federal University of Technology—Paraná—Campus Campo Mourão—for the performed analyses. The authors also thank the "Laboratório Multiusuário da UTFPR Campus Londrina (LabMulti-LD)" for the analyses.

Conflicts of Interest: The authors declare no conflicts of interest.

Abbreviations

The following abbreviations are used in this manuscript:

PCE	Photoconversion Energy Efficiency
jsc	Short-Circuit Current
Voc	Open-Circuit Potential
FF	Fill Factor
DSSC	Dye-Sensitized Solar Cell
FTO	Fluorine-Doped Tin Oxide
Pin	Incident Power
AM	Air Mass
EIS	Electrochemical Impedance Spectroscopy

References

1. Kraidy, A.F.; Yapi, A.S.; Saint-Gregoire, P.; Vaillant-Roca, L.; Eke, S.; Mouangue, R.; Jamali, A.; Gagou, Y. Enhancement of Natural Dye-Sensitized Solar Cell Efficiency Through TiO_2 Hombikat UV100 and TiO_2 P25 Photoanode Optimization. *Processes* **2024**, *12*, 2481. [CrossRef]
2. Wazzan, N. Structural Engineering of π-Linker Aromaticity in Anthanthrene-Based Dyes with D–π–A Configuration: DFT Investigation to Enhance Charge Transfer in DSSCs. *Processes* **2025**, *13*, 418. [CrossRef]
3. Tractz, G.T.; Viomar, A.; Dias, B.V.; De Lima, C.A.; Banczek, E.P.; Da Cunha, M.T.; Antunes, S.R.M.; Rodrigues, P.R.P. Recombination study of dye sensitized solar cells with natural extracts. *J. Braz. Chem. Soc.* **2019**, *30*, 371–378. [CrossRef]
4. Tractz, T.; Staciaki, F.; Regina, S.; Antunes, M.; Banczek, P.; Taras, M.; Rog, P. Nb_2O_5 synthesis and characterization by Pechini method to the application as electron transport material in a solar device. *Solar Energy* **2021**, *216*, 1–6. [CrossRef]
5. Larsson, L.F.G.; Arielo, G.; Maia, R.G.T.T.; Cristina, D.; Oliszeski, S.; Helleis, R. Application of Zinc Oxide in Hybrid Solar Cells Using a P3HT and P3OT Polymer Junction as Charge Carrier. *Mater. Res.* **2019**, *22*, e20180820. [CrossRef]
6. Tractz, T.; Viomar, A.; Dias, B.V.; Rodrigues, P.R.P. Photoelectrochemical Behavior of the Cell FTO/TiO_2/CeO_2/N719 Obtained from the Pechini and Precipitation of Cerium Oxide Methods. *J. Electron. Mater.* **2018**, *47*, 5556–5563. [CrossRef]
7. Lü, X.; Mou, X.; Wu, J.; Zhang, D.; Zhang, L.; Huang, F.; Xu, F.; Huang, S. Improved-Performance Dye-Sensitized solar cells using Nb-Doped TiO_2 electrodes: Efficient electron Injection and transfer. *Adv. Funct. Mater.* **2010**, *20*, 509–515. [CrossRef]
8. Hossain, M.I.; Aissa, B.; Khandakar, A.; Thomas, K.; Rahman, A.; Mansour, S. Exploring the optical and morphological properties of metal oxide thin films produced via reactive electron beam evaporation. *Cogent Eng.* **2024**, *11*, 2338144. [CrossRef]
9. Hossain, M.I.; Alharbi, F.H.; Tabet, N. Copper oxide as inorganic hole transport material for lead halide perovskite based solar cells. *Sol. Energy* **2015**, *120*, 370–380. [CrossRef]

10. Haque, M.M.; Mahjabin, S.; Abdullah, H.B.; Akhtaruzzaman, M.; Almohamadi, H.; Islam, M.A.; Hossain, M.I.; Ibrahim, M.A.; Chelvanathan, P. Exploring the theoretical potential of tungsten oxide (WOx) as a universal electron transport layer (ETL) for various perovskite solar cells through interfacial energy band alignment modulation. *J. Phys. Chem. Solids* **2025**, *196*, 112324. [CrossRef]
11. Hossain, M.I.; Al Kubaisi, G.; Aïssa, B.; Mansour, S. Probing the hydrophilic behaviour of e-beam evaporated silica thin films for PV-soiling application. *Mater. Sci. Technol.* **2022**, *38*, 753–759. [CrossRef]
12. Hossain, M.I.; Chelvanathan, P.; Aissa, B.; Khandakar, A.; Rahman, A.; Mansour, S. Enhanced perovskite solar cells performance with TiOx and SnOx thin films as electron transport layers. *Sci. Rep.* **2025**, *15*, 7709. [CrossRef] [PubMed]
13. Hossain, M.I.; Tong, Y.; Shetty, A.; Mansour, S. Probing the degradation pathways in perovskite solar cells. *Sol. Energy* **2023**, *265*, 112128. [CrossRef]
14. Hossain, M.I.; Chelvanathan, P.; Khandakar, A.; Thomas, K.; Rahman, A.; Mansour, S. Enhanced efficiency of bifacial perovskite solar cells using computational study. *Sci. Rep.* **2024**, *14*, 12984. [CrossRef]
15. Raba-Páez, A.M.; Suarez-Ballesteros, D.N.; Martínez-Zambrano, J.J.; Rojas-Sarmiento, H.A.; Rincón-Joya, M. Pechini method used in the obtention of semiconductor nanoparticles based niobium. *Dyna* **2015**, *82*, 52–58. [CrossRef]
16. Guimaraes, R.R.; Parussulo, A.L.A.; Araki, K. Impact of nanoparticles preparation method on the synergic effect in anatase/rutile mixtures. *Electrochim. Acta* **2016**, *222*, 1378–1386. [CrossRef]
17. Guimaraes, R.R.; Parussulo, A.L.A.; Toma, H.E.; Araki, K. New tunable ruthenium complex dyes for TiO_2 solar cells. *Inorganica Chim. Acta* **2013**, *404*, 23–28. [CrossRef]
18. Tractz, G.T.; Antunes, S.R.M.; Rodrigues, P.R.P. Nb/TiO_2 oxides: A study of synthesis and electron transport mechanism as an ETL in a solar device. *J. Photochem. Photobiol. A Chem.* **2023**, *444*, 114899. [CrossRef]
19. Maia, P.R.P.R.G.A.R.; Larsson, L.F.G.; Viomar, A.; Maia, E.C.R.; de Santana, H. Aperfeiçoamento da produção de partículas de óxido de zinco para aplicação em células solares. *Cerâmica* **2016**, *62*, 91–97. [CrossRef]
20. Maia, G.A.R.; Larsson, L.F.G.; Viomar, A.; Matos, L.A.C.; Antunes, S.R.M.; Maia, E.C.R.; Oliveira, M.F.; Cunha, M.T.; Rodrigues, P.R.P. Influence of zinc oxide morphology in hybrid solar cells of poly(3-octylthiophene). *J. Mater. Sci. Mater. Electron.* **2016**, *27*, 8271–8278. [CrossRef]
21. Vanlaeke, P.; Swinnen, A.; Haeldermans, I.; Vanhoyland, G.; Aernouts, T.; Cheyns, D.; Deibel, C.; D'Haen, J.; Heremans, P.; Poortmans, J.; et al. P3HT/PCBM bulk heterojunction solar cells: Relation between morphology and electro-optical characteristics. *Sol. Energy Mater. Sol. Cells* **2006**, *90*, 2150–2158. [CrossRef]
22. Jarzynska, K.; Ciura, K.; Gao, X.J.; Mikolajczyk, A.; Gao, X.; Puzyn, T. Understanding the zeta potential of nanomaterials through predictive nanoinformatics. *Nano Today* **2025**, *64*, 102783. [CrossRef]
23. Hagfeldt, A.; Boschloo, G.; Sun, L.; Kloo, L.; Pettersson, H. Dye-Sensitized Solar Cells. *Chem. Rev.* **2010**, *110*, 6595–6663. [CrossRef]
24. Eblagon, K.M.; Malaika, A.; Ptaszynska, K.; Pereira, M.F.R.; Figueiredo, J.L. Impact of thermal treatment of Nb_2O_5 on its performance in glucose dehydration to 5-hydroxymethylfurfural in water. *Nanomaterials* **2020**, *10*, 1685. [CrossRef]
25. O'Regan, B.; Grätzel, M. A low-cost, high-efficiency solar cell based on dye-sensitized colloidal TiO_2 films. *Nature* **1991**, *353*, 737–740. [CrossRef]
26. Grätzel, M. Photoelectrochemical cells. *Nature* **2001**, *414*, 338–344. [CrossRef]
27. Sathasivam, S.; Williamson, B.A.D.; Althabaiti, S.A.; Obaid, A.Y.; Basahel, S.N.; Mokhtar, M.; Scanlon, D.O.; Carmalt, C.J.; Parkin, I.P. Chemical Vapor Deposition Synthesis and Optical Properties of Nb_2O_5 Thin Films with Hybrid Functional Theoretical Insight into the Band Structure and Band Gaps. *ACS Appl. Mater. Interfaces* **2017**, *9*, 18031–18038. [CrossRef]
28. Sultana, R.; Islam, K.; Chakraborty, S. Tuning Optical and Electrochemical Properties of Nb_2O_5 Thin Films via WO_3 Doping. *Trans. Electr. Electron. Mater.* **2025**, *26*, 48–59. [CrossRef]
29. Chaiworn, P.; Teerananattapong, W.; Reunchan, P.; Tubtimtae, A.; Wongrat, E. Effect of tungsten oxide concentration on structural, morphological, compositional, dispersion energy, and linear/nonlinear optical properties of niobium pentoxide thin films. *Opt. Mater.* **2025**, *161*, 116807. [CrossRef]
30. Longo, C.; De Paoli, M.A. Dye-Sensitized Solar Cells: A Successful Combination of Materials. *J. Braz. Chem. Soc.* **2003**, *14*, 889–901. [CrossRef]
31. Wu, J.J.; Chen, G.R.; Yang, H.H.; Ku, C.H.; Lai, J.Y. Effects of dye adsorption on the electron transport properties in ZnO-nanowire dye-sensitized solar cells. *Appl. Phys. Lett.* **2007**, *90*, 2007–2009. [CrossRef]
32. Kim, T.Y.; Kim, J.H.; Kim, H.B.; Park, K.H.; Lee, J.W.; Cho, S.Y. Adsorption and kinetics properties of TiO_2 photoelecrode using natural paprika oleoresin (*Capsicum annuum* L.) dye for dye-sensitized solar cells. *Int. J. Electrochem. Sci.* **2018**, *13*, 3935–3947. [CrossRef]
33. Ramasamy, E.; Lee, J. Ordered mesoporous SnO_2-based photoanodes for high-performance dye-sensitized solar cells. *J. Phys. Chem. C* **2010**, *114*, 22032–22037. [CrossRef]
34. Valerio, T.; Arielo, G.; Maia, R.; Fernanda, L. Study of the Nb_2O_5 Insertion in ZnO to Dye-sensitized Solar Cells 2. Material and Methods. *Mater. Res.* **2019**, *22*, 1–5. [CrossRef]

35. Valerio, T.L.; Tractz, G.; Maia, G.A.R.; Banczek, E.D.P.; Rodrigues, P.R.P. Minimizing of charge recombination by Nb2O5 addition in dye-sensitized solar cells. *Opt. Mater.* **2020**, *109*, 110310. [CrossRef]
36. de Lima, A.A.; Tractz, G.T.; Macedo, A.G.; Thomazi, F.; Rodrigues, P.R.P.; Dartora, C.A. Electrochemical investigation of PEDOT:PSS and Nb_2O_5 composites as counter electrodes for dye-sensitized solar cells. *Opt. Mater.* **2022**, *132*, 112763. [CrossRef]
37. Yang, J.H.; Bark, C.W.; Kim, K.H.; Choi, H.W. Characteristics of the dye-sensitized solar cells using TiO_2 nanotubes treated with $TiCl_4$. *Materials* **2014**, *7*, 3522–3532. [CrossRef]
38. Bard, A.J.; Faulkner, L.R. *Electrochemical Methods: Fundamentals and Applications*, 2nd ed.; Jonh Wiley & Sons, Inc.: New York, NY, USA, 2000.
39. Liberatore, M.; Decker, F.; Burtone, L.; Zardetto, V.; Brown, T.M.; Reale, A.; Di Carlo, A. Using EIS for diagnosis of dye-sensitized solar cells performance. *J. Appl. Electrochem.* **2009**, *39*, 2291–2295. [CrossRef]
40. Gratzel, M.; Wang, Q.; Moser, J.E. Electrochemical impedance spectroscopic analysis of dye-sensitized solar cells. *J. Phys. Chem. B* **2005**, *109*, 14945–14953. [CrossRef]
41. Tractz, G.T.; Dias, B.V.; Banczek, E.P.; da Cunha, M.T.; Alves, G.J.T.; Rodrigues, P.R.P. Dye Sensitized Solar Cells (CSSC): Perspectives, Materials, Functioning and Characterization Techniques. *Rev. Virtual De. Química* **2020**, *12*, 748–774. [CrossRef]
42. Bisquert, J.; Fabregat-santiago, F. Electron Lifetime in Dye-sensitized solar cells: Theory and Interpretation of Measurements. *J. Phys. Chem. C* **2009**, *113*, 17278–17290. [CrossRef]
43. Camargo Matheus, A.P.; Gonçalves Larsson, L.F.; Tractz, G.T.; Pinto Rodrigues, P.R. The TiO_2/electrolyte interface in DSSCs: An electrochemical study of the insertion of BTAH, BZM, and indole. *Opt. Mater.* **2025**, *159*, 116637. [CrossRef]
44. Rigueira, R.F.; Tractz, G.T.; Barancelli, D.A. Fabrication of a dye sensitized solar cell using TiO_2 sensitized with a mono-carbonyl curcumin analog. *J. Iran. Chem. Soc.* **2024**, *21*, 2095–2101. [CrossRef]
45. Bisquert, J.; Fabregat-Santiago, F. *Impedance Spectroscopy: A General Introduction and Application to Dye-Sensitized Solar Cells*, 1st ed.; EPFL Press: Lausanne, Switzerland, 2010.

Disclaimer/Publisher's Note: The statements, opinions and data contained in all publications are solely those of the individual author(s) and contributor(s) and not of MDPI and/or the editor(s). MDPI and/or the editor(s) disclaim responsibility for any injury to people or property resulting from any ideas, methods, instructions or products referred to in the content.